Spectroscopic and Theoretical Study of the Molecular and Electronic Structures of a Terthiophene-Based Quinodimethane

ARTICLE *in* CHEMPHYSCHEM · APRIL 2004

Impact Factor: 3.42 · DOI: 10.1002/cphc.200300963 · Source: PubMed

Spectroscopic and Theoretical Study of the Molecular and Electronic Structures of a Terthiophene-Based Quinodimethane

Juan Casado,[a] Ted M. Pappenfus,[b] Kent R. Mann,[b] Enrique Ortí,*[c] Pedro M. Viruela,[c] Begoña Milián,[c] Víctor Hernández,[a] and Juan T. López Navarrete*[a]

The UV/Vis, infrared absorption, and Raman scattering spectra of 3′,4′-dibutyl-5,5′′-bis(dicyanomethylene)-5,5′′-dihydro-2,2′:5′,2′′-terthiophene have been analyzed with the aid of density functional theory calculations. The compound exhibits a quinoid structure in its ground electronic state and presents an intramolecular charge transfer from the terthiophene moiety to the $C(CN)_2$ groups. The molecular system therefore consists of an electron-deficient terthiophene backbone end-capped with electron-rich $C(CN)_2$ groups. The molecule is characterized by a strong absorption in the red, due to the HOMO→LUMO $\pi-\pi^*$ electronic transition of the terthiophene backbone that shifts hypsochromically on passing from the solid state to solution and with the polarity of the solvent. The analysis of the vibrational spectra confirms the structural conclusions and supports the existence of an intramolecular charge transfer. Vibrational spectra in several solvents and as a function of temperature have also been studied. Significant frequency upshifts of the vibrations involved in the π-electron-conjugated pathway have been noticed upon solution in polar solvents and with the lowering of the temperature. Finally, we propose a quinoid molecule as a reliable structural and electronic model for dication species in doped oligothiophenes or for bipolaron charged defects in doped polythiophene.

1. Introduction

Conjugated oligothiophenes are currently receiving much attention as organic semiconductors for electronic devices such as field-effect transistors (FETs).[1, 2] Oligothiophenes typically behave as p-type conductors or hole-transporting materials. n-Type or electron-transporting oligothiophenes, however, are also of great interest for the fabrication of p – n heterojunctions and complementary circuits. The operating properties of these organic-based devices depend on the charge-transport properties, which are closely related to the energies of the HOMO and the LUMO that govern charge injection, and to the splitting of these levels in the solid state (due to intermolecular interactions), which determines charge mobility.[3, 4] The strength of the electronic coupling between the HOMO levels controls the hole transport and that between the LUMO levels modulates the electron transport. Therefore, charge-transfer processes and intermolecular interactions are key topics to be investigated for the development of these materials.

Recently, thin-film transistors (TFTs) based on 3′,4′-dibutyl-5,5′′-bis(dicyanomethylene)-5,5′′-dihydro-2,2′:5′,2′′-terthiophene [$Bu_2(DCM)_2Tth$, Figure 1] have been reported.[5–7] The initial report shows that this molecule works very efficiently as n-channel semiconductor, which, as mentioned above, is somewhat rare for this class of compounds.[6] Quinoid oligothiophenes have a HOMO – LUMO energy gap inherently smaller than that of conventional aromatic oligothiophenes, which makes ambipolar (both p- and n-type) transport more likely because smaller gate voltages are required to populate the HOMO and LUMO levels (valence and conduction bands) with charge carriers. In fact, within the course of this investigation, the group at the University of Minnesota successfully achieved ambipolar transport in a TFT using $Bu_2(DCM)_2Tth$ as the semiconducting layer.[7] Ambipolar behavior in organic-based transistors is rare and, to the best of our knowledge, the case of $Bu_2(DCM)_2Tth$ represents the first example of ambipolar transport in a TFT device based on a single conjugated organic

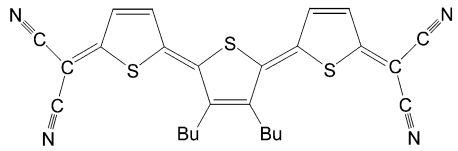

Figure 1. *Chemical structure of $Bu_2(DCM)_2Tth$.*

[a] *Dr. J. Casado, Prof. Dr. V. Hernández, Prof. Dr. J. T. López Navarrete*
Departamento de Química Física, Universidad de Málaga
29071 Málaga (Spain)
E-mail: teodomiro@uma.es

[b] *Dr. T. M. Pappenfus, Prof. Dr. K. R. Mann*
Department of Chemistry, University of Minnesota
Minneapolis, MN 55455 (USA)

[c] *Prof. Dr. E. Ortí, Prof. Dr. P. M. Viruela, B. Milián*
Institut de Ciència Molecular, Universitat de València
46100 Burjassot (València) (Spain)
Fax: + (34)-963543156
E-mail: enrique.orti@uv.es

 DOI: 10.1002/cphc.200300963

semiconductor material. The electron field-effect mobilities measured for vapor- and solution-deposited films of $Bu_2(DCM)_2Tth$ were 0.005 and 0.002 $cm^2V^{-1}s^{-1}$, respectively.[6] These values have been improved up to 0.2 $cm^2V^{-1}s^{-1}$,[7] [very close to the highest electron mobility of 0.6 $cm^2V^{-1}s^{-1}$ reported so far for an organic TFT (OTFT)].[8] These relatively high carrier mobilities are accounted for by the effectiveness of the intermolecular interactions, which determine the splitting of the HOMO and LUMO levels.

Infrared and Raman spectroscopies have proven to be useful techniques in obtaining fundamental information on molecular structures and molecular interactions. Vibrational analysis uses the normal modes of a molecule as microscopic probes of its structure. Vibrational spectra can, therefore, provide valuable information on fundamental characteristics of $Bu_2(DCM)_2Tth$ such as the interactions between the different structural moieties that constitute the molecule (cyano, terthiophene, and butyl groups), the molecular conformation, and the intermolecular interactions in solid state as well as in solution. To evaluate this information, one first needs a molecular model that allows the establishment of a reliable relationship between the vibrational spectra of the conjugated molecule and its electronic structure. We will make use of the widely accepted effective conjugation coordinate (ECC) model developed by Zerbi et al.[9–11] All previous data obtained from the analysis of the vibrational properties of similar molecules is also highly desirable for comparison purposes. Fortunately, vibrational data are, at present, available for a large number of aromatic and quinoid oligothiophenes.[12–18]

The outstanding charge-transport properties of $Bu_2(DCM)_2Tth$ demonstrate that quinoidal oligothiophenes represent a new class of semiconductors with promising device applications. This Article focuses on the analysis of the molecular structure and electronic properties of $Bu_2(DCM)_2Tth$ by using a combination of electronic and vibrational spectroscopies together with density functional theory (DFT) calculations. Both intra- and intermolecular interactions will be addressed with the help of the spectra recorded in solid state, in solution, and also as a function of temperature.

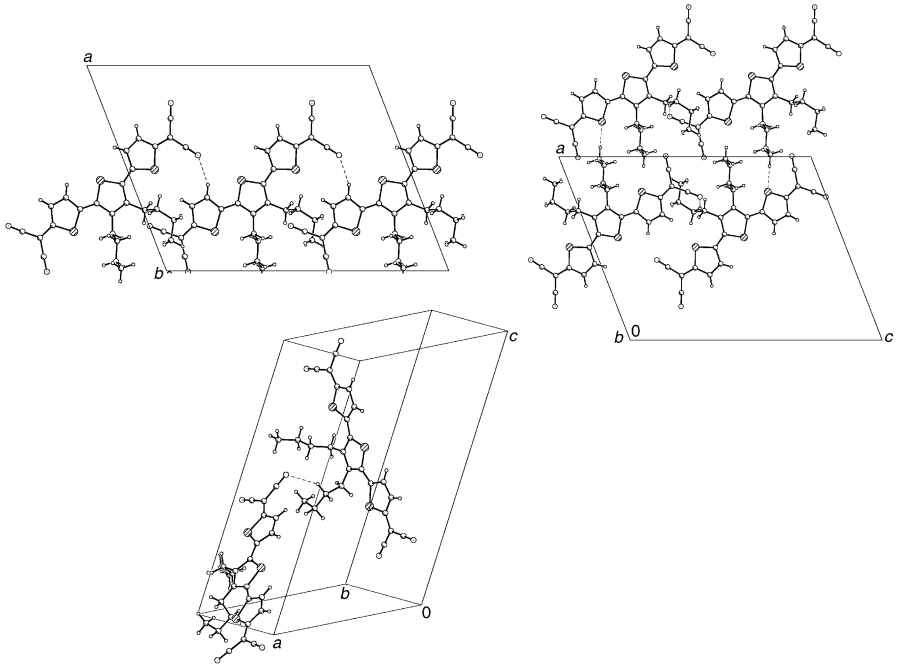

Figure 2. *Packing views along different crystal axes showing unconventional intermolecular interactions (dotted lines).*[5]

2. Results and Discussion

Crystallographic and Molecular Structures

The crystal structure of $Bu_2(DCM)_2Tth$ has been previously reported and reveals that the molecules pack face-to-face along the *b* axis forming π stacks of π dimers.[5, 6] Figure 2 displays the organization of the $Bu_2(DCM)_2Tth$ molecules along different axes of the unit cell. Three intermolecular interactions, longer than typical hydrogen bonds,[19] are present in the crystal packing. The shortest intermolecular interaction corresponds to a CN···H-(thienyl) contact (2.355 Å) between molecules in adjacent stacks along the *c* axis. In addition, CN···H(butyl) and S···H(butyl) intermolecular interactions occur at distances of 2.561 and 2.923 Å, respectively. The role of these interactions in understanding the vibrational properties is discussed below.

B3LYP/6-31G** calculations predict a fully planar structure for $Bu_2(DCM)_2Tth$ with a transoid configuration of the sulfur atoms in adjacent thiophene rings and the butyl chains pointing out of the molecular plane. The theoretical structure is in good agreement with that observed in the crystal with the exception of the orientation of the butyl chains. In the crystal, both chains project out of the molecular plane in the same direction, which gives rise to a C_s-type molecular structure. Theoretically, the minimum-energy structure corresponds to a C_2 conformation, in which the butyl chains lie above and below the molecular plane, thus minimizing their steric interactions. The C_s-type structure is observed in the crystal because it is only 0.68 kcal mol^{-1} less stable than the C_2 form and leads to a more compact crystal packing. Since calculations performed for both structures predict negligible differences in geometrical parameters, vibrational frequencies, and electronic properties, only the results obtained for the C_2 structure are quoted below.[20]

Figure 3 compares the bond distances obtained experimentally from X-ray analysis with those calculated theoretically at the B3LYP/6-31G** level. The terthiophene moiety bears a quinoid structure, in which the shortest carbon – carbon (CC) distances correspond to the C_β–C_β bonds of the thiophene rings, to the inter-ring C_α–$C_{\alpha'}$ bonds, and to the bonds that connect the

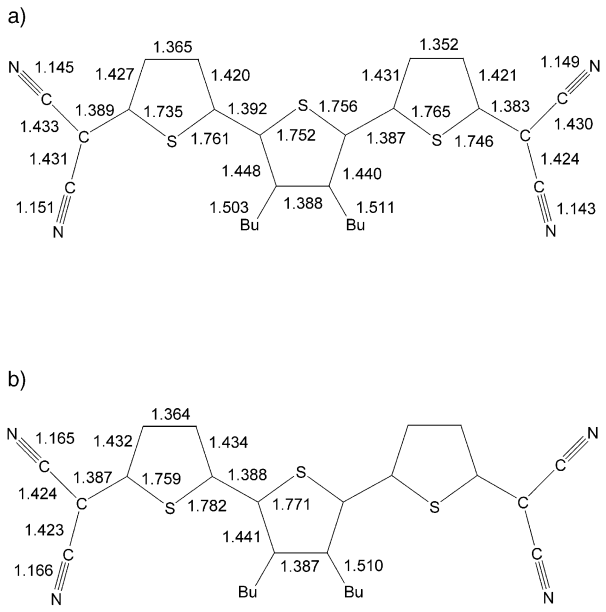

Figure 3. *Bond lengths (in Å) of $Bu_2(DCM)_2Tth$. a) Experimental values from X-ray analysis.[5] b) B3LYP/6-31G**-optimized values (C_2 symmetry).*

oligothiophene unit to the dicyanomethylene groups. The terthiophene backbone thus exhibits a reversal of the single–double bond alternation pattern with respect to that commonly observed for aromatic α,α′-oligothiophenes, for which the C_β–C_β bonds and the C_α–$C_{\alpha'}$ bonds are longer than the C_α–C_β bonds.[21–23] The quinoid structure of $Bu_2(DCM)_2Tth$ is, in fact, similar to that predicted theoretically for aromatic oligothiophenes in the dication or bipolaron state.[24]

The attachment of the butyl chains to the central thiophene ring changes the structure of this ring compared to that of the outer thiophene rings. Thus, alkyl substitution determines that the C_α–C_β and C_β–C_β bonds of the central ring are longer than the respective bonds of the outer rings (see Figure 3). Moreover, the single–double C-C bond length alternation (BLA) is somewhat smaller for the central ring (X-ray: 0.056 Å; B3LYP/6-31G**: 0.054 Å) than for the outer rings (average X-ray value: 0.066 Å; B3LYP/6-31G**: 0.069 Å). This is not the case for the unsubstituted molecule, 5,5′′-bis(dicyanomethylene)-5,5′′-dihydro-2,2′:5′,2′′-terthiophene [$(DCM)_2Tth$], for which almost identical BLA values are calculated at the B3LYP/6-31G** level for the central (0.066 Å) and for the outer (0.068 Å) rings. The *n*-butyl substituents therefore introduce a slight alteration in the conjugation path. The effect of the substituents is discussed below on the light of the vibrational spectra.

The agreement between the solid-state X-ray data and the B3LYP/6-31G**-optimized bond lengths is within 0.01 Å for the C-C bonds. However, for the C–S and C≡N bonds, this agreement is not as good. In these cases, the optimized bond lengths overestimate the X-ray values by ≈0.02 Å. In the case of the C–S bonds, the overestimation is due to a limitation of the theoretical approach, since the B3LYP functional is known to yield too long C–S distances.[25] For the C≡N bonds, the B3LYP functional has been shown to provide bond lengths in good accordance with gas-phase data, while the X-ray values seem to be underestimated.[26] The X-ray molecular structure furthermore reveals noticeable bond length asymmetries concerning the outer thiophene rings and the cyano groups. These asymmetries are probably due to the different molecular environment in the crystal and are not reproduced by the calculations because they are performed for the isolated molecule. Polar cyano groups are known to promote extensive interactions between adjacent molecules in the crystal. These interactions have significant effects on the electronic and vibrational properties of $Bu_2(DCM)_2Tth$ as addressed below.

The B3LYP/6-31G** net atomic charges, calculated using Mulliken population analysis, indicate that each dicyanomethylene group supports a negative charge of −0.29e, which is balanced by the outer rings (+0.19e) and the central ring (+0.20e). An electron-density transfer from the central terthiophene moiety, which acts as an electron donor, to the electron-withdrawing $C(CN)_2$ groups therefore takes place in the electronic ground state of $Bu_2(DCM)_2Tth$. This intramolecular charge transfer gives rise to an electron-deficient oligothiophene backbone.

Electronic Absorption Spectra

Figure 4 shows the UV/Vis spectra recorded for $Bu_2(DCM)_2Tth$ in the solid state, as well as in CS_2, CH_2Cl_2, and CH_3CN solutions. The spectra exhibit an intense and broad band in the range 500–850 nm, with a maximum at 700 nm (1.77 eV) in the solid state.

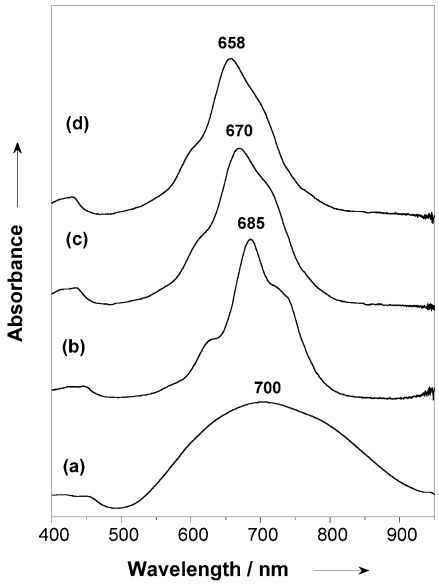

Figure 4. *UV/Vis spectra of $Bu_2(DCM)_2Tth$ recorded in solid state (a), in CS_2 (b), in CH_2Cl_2 (c), and in CH_3CN (d).*

This band is largely red-shifted with respect to the electronic π–π* absorptions observed for aromatic oligothiophenes in the visible region. In α,α′-oligothiophenes, the maximum absorption appears at 355 nm (3.49 eV) for terthiophene and shifts to 432 nm (2.87 eV) for sexithiophene.[27] The $C(CN)_2$ groups in

$Bu_2(DCM)_2Tth$ also participate in the π electron system, but the extension of the π-conjugation path to these groups does not explain the long wavelength recorded for this terthiophene. For the unsubstituted $(DCM)_2Tth$ trimer, the maximum of the absorption band is observed at 646 nm (1.92 eV) in the solid state.[12a] Butyl substitution of the $(DCM)_2Tth$ trimer therefore gives rise to a red shift of 54 nm. This bathochromic shift has not been previously detected for the corresponding thiophene-based quinodimethane monomer and dimer, for which hexyl substitutions only affect the maximum absorption wavelength by a few nanometers.[28]

To investigate the nature of the electronic transitions that give rise to the absorption bands observed experimentally, the lowest-energy electronic excited states of $Bu_2(DCM)_2Tth$ and $(DCM)_2Tth$ were calculated using the time-dependent density functional theory (TDDFT) approach and the B3LYP/6-31G**-optimized geometries. Theoretical calculations predict only one intense electronic transition in the visible region (below 3.0 eV). The transition corresponds to the excitation to the first excited singlet electronic state (S_1) and implies a one-electron promotion from the highest occupied molecular orbital (HOMO) to the lowest unoccupied molecular orbital (LUMO). The intense absorption band observed experimentally around 700 nm is, therefore, assigned to the $S_0 \rightarrow S_1$ electronic transition, which has been computed at almost identical energies for $Bu_2(DCM)_2Tth$ (1.96 eV, 635 nm) and $(DCM)_2Tth$ (1.97 eV, 630 nm), and with similar oscillation strengths ($f = 1.67$ and 1.74, respectively). The calculated excitation energies are in good agreement with the experimental values but do not reproduce the red shift observed experimentally upon butyl substitution.

Figure 5 shows the atomic orbital composition calculated for the HOMO and the LUMO of $Bu_2(DCM)_2Tth$. Both orbitals are of π nature, as expected, and spread over the whole π-conjugated backbone with contributions from the nitrogen atoms. The topologies of the HOMO and the LUMO are reversed with respect to those observed for aromatic oligothiophenes due to the quinoid structure of the terthiophene skeleton. This reversal determines that the HOMO – LUMO energy gaps of 1.62 eV, calculated at the B3LYP/6-31G** level for $Bu_2(DCM)_2Tth$ and $(DCM)_2Tth$, are much lower than that obtained for aromatic terthiophene (3.45 eV) at the same computational level. The low energy of the electronic absorption observed in the visible region therefore arises from the heteroquinoid structure of the molecule. The topologies of the HOMO and the LUMO show that this absorption originates in the $\pi - \pi^*$ transition of the terthiophene backbone. No significant intramolecular charge transfer to the dicyanomethylene groups is detected, since the two dicyanomethylene groups equally participate in both frontier orbitals. The applicability of the TDDFT approach to donor – acceptor systems has been questioned in the literature, because it leads to large deviations for the excitation energies of charge-transfer states.[29] However, this is not a general rule,[30] and it does not particularly affect the assignment of the HOMO $\rightarrow$LUMO transition of $Bu_2(DCM)_2Tth$, since this transition shows no significant charge-transfer character.

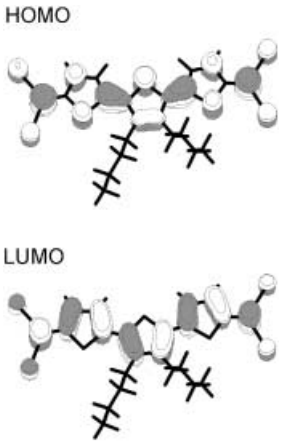

Figure 5. *Electron density contours (0.03 e bohr^{-3}) calculated using the MOLDEN graphics interface for the HOMO and LUMO of $Bu_2(DCM)_2Tth$ at the B3LYP/6-31G** level.*

The absorption spectrum in CS_2 solution shows a maximum at 685 nm (1.81 eV) with shoulders both on the lower and on the higher energy sides. The shoulders are assigned to vibronic components of the HOMO $\rightarrow$LUMO transition, since no other electronic transition is calculated to occur below 3 eV. Vibronic structure is usually observed for the $S_0 \rightarrow S_1$ band in aromatic oligothiophenes.[31] The spectra in CH_2Cl_2 and CH_3CN solutions display similarly structured bands with maxima at 670 nm (1.85 eV) and at 656 nm (1.89 eV), respectively. A blue shift of 44 nm is therefore measured from the solid state to the acetonitrile solution. In view of the small dielectric constant of CS_2 ($\varepsilon = 2.61$), the shift from 700 (solid) to 685 nm (CS_2) can be reasonably related with the splitting of the HOMO and LUMO levels in the solid state due to intermolecular interactions. The shift from 685 (CS_2) to 656 nm (CH_3CN) should be explained in terms of interactions with the solvent molecules, which can influence the charge transfer that takes place in the ground state from the terthiophene backbone to the $C(CN)_2$ groups.

$Bu_2(DCM)_2Tth$ and other related oligothienoquinoid systems[12, 27, 32, 33] can be viewed as structural and electronic models of dication species in oxidized oligothiophenes. Oxidation of aromatic oligothiophenes leads to the appearance of quinoid structures growing up from the center of the oligothiophene chain at the expense of the aromatic structure. The quinoid structure of the dication or bipolaron species has been shown to extend over the whole oligothiophene backbone for oligomers such as end-capped α,α'-quaterthiophenes and sexithiophenes.[18] The electronic spectra of these dications are characterized by an intense absorption band at low energies (quaterthiophenes $\approx$750 – 800 nm, sexithiophenes $\approx$950 – 1100 nm)[18, 31a, 34] that can be correlated with the intense band observed here for the $Bu_2(DCM)_2Tth$ trimer at 700 nm.

Infrared Spectrum in the High Energy Region

Figure 6 displays the infrared spectra recorded for $Bu_2(DCM)_2Tth$ as a pure solid and in CCl_4 solution in the 3200 – 2800 cm^{-1} range. The spectra show three double-peak structures almost at the same frequencies for both the liquid and the solid phases but with different relative intensities. The infrared bands at 3085

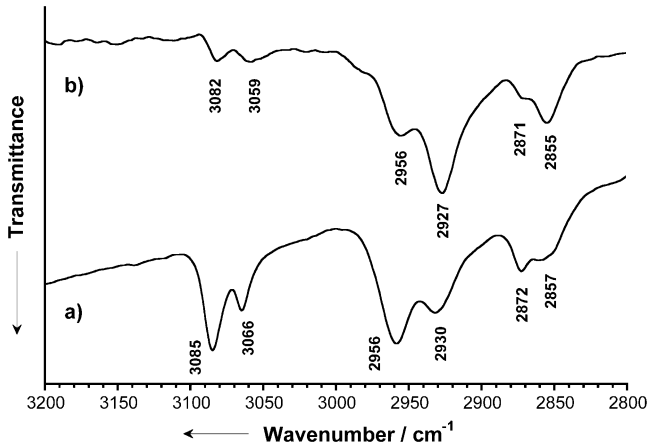

Figure 6. FT-Infrared spectrum of $Bu_2(DCM)_2Tth$ in solid state (a) and in CCl_4 solution (b) over probe energies of 3200 – 2800 cm^{-1}.

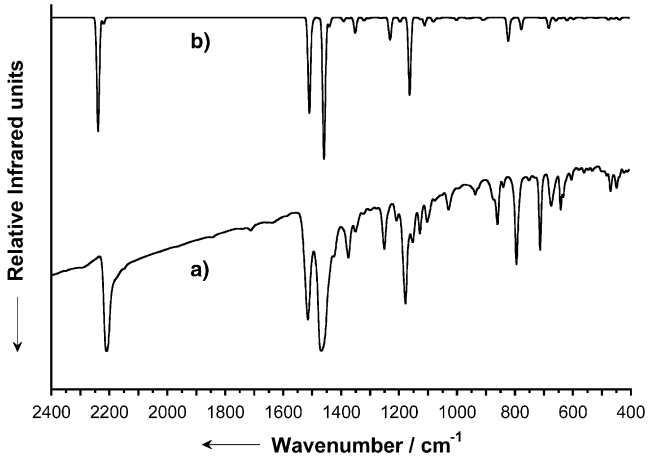

*Figure 7. FTIR spectrum of $Bu_2(DCM)_2Tth$ over probe energies of 2400 – 400 cm^{-1}. (a) Experimentally recorded in solid state. (b) Theoretically calculated (B3LYP/6-31G**). The intensity of the most intense theoretical band at 1460 cm^{-1} has been scaled by a factor of 0.4.*

and 3066 cm^{-1} correspond to the C—H stretching vibrations, $\tilde{\nu}$(C—H), of the thienyl rings.[14, 15] B3LYP calculations predict the double-peak structure (3117 and 3094 cm^{-1}) and assign the band at 3085 cm^{-1} to the stretching of the C—H bonds adjacent to the $C(CN)_2$ groups, while the band at 3066 cm^{-1} is due to the innermost C—H bonds. In the solid state, the latter bonds interact with the CN groups of the adjacent molecules (see Figure 2). This interaction hinders the C—H stretching, which requires more energy for the vibration, thus explaining the upshift from 3059 cm^{-1} in solution to 3066 cm^{-1} in the solid.

The two doublets in the 3000 – 2800 cm^{-1} range correspond to the stretching vibrations of the aliphatic C—H bonds of the butyl groups.[14, 15] The band at 2956 cm^{-1} (calculated at 2991 cm^{-1}) mainly originates in the antisymmetric stretching vibration of the CH_3 groups, while that at 2930 cm^{-1} (calculated at 2949 cm^{-1}) is due to the antisymmetric stretching vibration of the CH_2 groups. The bands at 2872 and 2857 cm^{-1} (calculated at 2920 and 2906 cm^{-1}) result from the symmetric stretching of the CH_3 and CH_2 groups, respectively. The bands at 2956 and 2872 cm^{-1} therefore imply the vibration of the terminal CH_3 groups, and increase their relative intensity in the solid state.

Infrared Spectrum in the Mid – Low Energy Region

The Fourier transform infrared spectrum recorded for $Bu_2(DCM)_2Tth$ in the 2500 – 400 cm^{-1} energy range is shown in Figure 7 together with the theoretical spectrum calculated at the B3LYP/6-31G** level. Figure 8 depicts the eigenvectors (atomic vibrational displacements) calculated for the normal modes associated with the most important IR bands. The theoretical spectrum nicely reproduces the shape and position of the experimental features but seems to fail in predicting the relative intensities. Nevertheless, when experimental spectra recorded on solid samples are compared with theoretical data evaluated on isolated entities, it should be taken into account that solid state intermolecular interactions can influence the relative intensities of the vibrational bands and provoke the splitting of the specific bands into structured peaks.

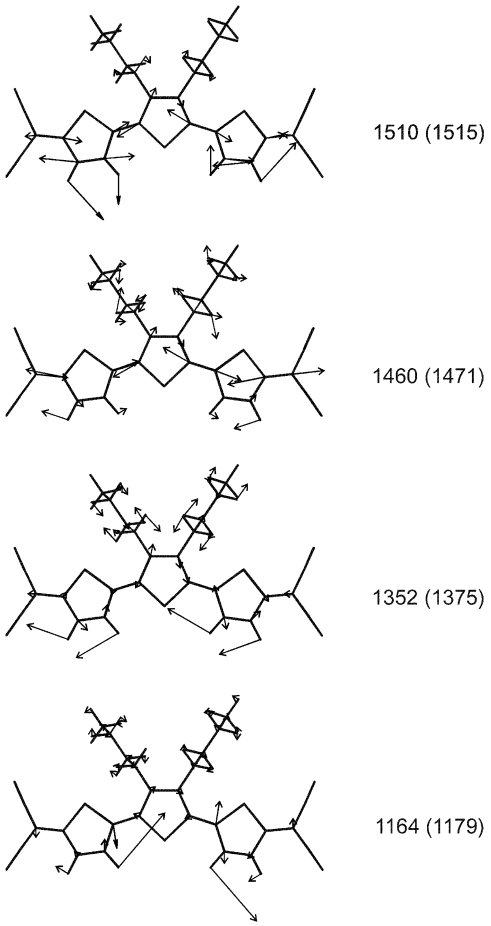

*Figure 8. B3LYP/6-31G** eigenvectors calculated for selected infrared bands of $Bu_2(DCM)_2Tth$. Scaled and experimental (in parentheses) wavenumbers are given in cm^{-1}.*

The $\tilde{\nu}$(C≡N) vibration is measured as an intense band at 2210 cm^{-1} with a shoulder at 2178 cm^{-1}. The strongest absorption corresponds to the antisymmetric normal mode calculated

at 2239 cm^{-1}, in which the two CN bonds of each $C(CN)_2$ group vibrate in-phase. The shoulder is assigned to the symmetric mode (2220 cm^{-1}), in which the CN bonds of each $C(CN)_2$ group vibrate out-of-phase.

The frequency of the $\tilde{\nu}$(C≡N) vibration (2210 cm^{-1}) is useful for estimating the degree of intramolecular charge transfer, since it is highly sensitive to the electron density borne by the CN triple bond. The frequency of this band downshifts on complexation with electron donors or upon reduction. For instance, the CN stretching band appears at 2225 cm^{-1} for neutral TCNQ (7,7,8,8-tetracyano-p-quinodimethane), at 2197 cm^{-1} for $TCNQ^-$, and at 2164 cm^{-1} for $TCNQ^{2-}$.[35, 36] Using these data to make a correlation between the $\tilde{\nu}$(C≡N) frequency and the net charge per $C(CN)_2$ group, the intramolecular charge transfer to each $C(CN)_2$ group in $Bu_2(DCM)_2Tth$ is estimated to be approximately 0.26*e*, in good accordance with the charge transfer calculated theoretically (0.29*e*).

The infrared spectrum over the 1600 – 1000 cm^{-1} range provides structural information about the π-conjugated oligothiophene backbone. The strongest IR band at 1471 cm^{-1} and the intense band at 1515 cm^{-1} are assigned to the normal modes calculated at 1460 and at 1510 cm^{-1}, respectively. As sketched in Figure 8, both modes describe antisymmetric stretching vibrations of the CC double bonds. The mode at 1510 cm^{-1} implies motions of the C_β=C_β bonds of the outer thiophene rings coupled with the inter-ring C_α=$C_{\alpha'}$ bonds and, in a low degree, with the terminal C_α=C_{sp^2} bonds connecting the rings to the $C(CN)_2$ groups. The mode at 1460 cm^{-1} involves motions of both the inter-ring C_α=$C_{\alpha'}$ and the end C_α=C_{sp^2} bonds. These two vibrations are recorded at 1528 and 1499 cm^{-1}, respectively, for the $(DCM)_2$Bth dimer and they also give rise to the two strongest IR features below 1600 cm^{-1}.[13a] The lower frequencies measured here for $Bu_2(DCM)_2Tth$ are due to the extension of the C-C π-conjugated pathway defined by the oligothiophene backbone.

The band at 1375 cm^{-1} (calculated 1352 cm^{-1}) is due to the antisymmetric stretching of the C_α–C_β bonds coupled with in-plane thienyl C–H deformations, δ(C–H), and aliphatic $\delta(CH_2)$ vibrations (see Figure 8). The band at 1349 cm^{-1} (calculated 1321 cm^{-1}) corresponds to a similar vibration but with a higher contribution from the central thiophene ring. The set of bands between that at 1251 cm^{-1} (calculated 1232 cm^{-1}) and that at 1029 cm^{-1} (calculated 1003 cm^{-1}) can be also described as skeletal stretching vibrations of the C–C bonds with large contributions from thienyl δ(C–H) and aliphatic $\delta(CH_2)$ modes. A typical eigenvector for these vibrations is that shown in Figure 8 for the normal mode calculated at 1164 cm^{-1}, which gives rise to the most intense peak in this region at 1179 cm^{-1}. Bands below 1000 cm^{-1} are usually related to a mixing of different in-plane vibrations or to out-of-plane bending and folding modes.

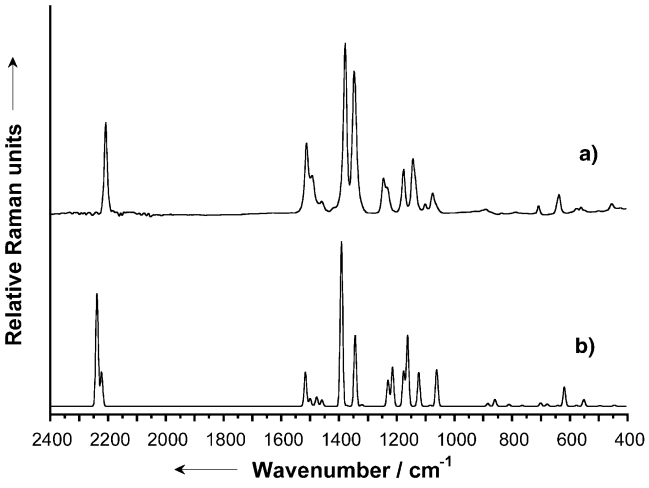

Figure 9. *FT-Raman spectrum of $Bu_2(DCM)_2Tth$ over probe energies of 2400 – 400 cm^{-1}. a) Experimentally recorded in solid state. b) Theoretically calculated (B3LYP/6-31G**). The intensity of the most intense theoretical band at 1393 cm^{-1} has been scaled by a factor of 0.2.*

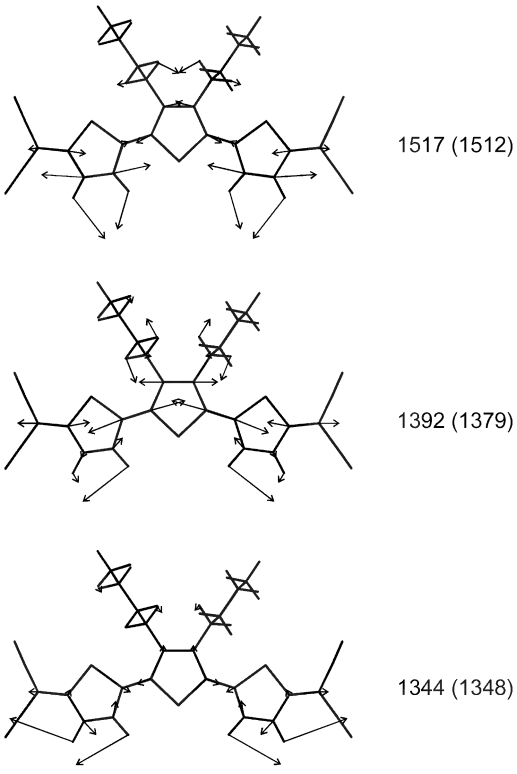

Figure 10. *B3LYP/6-31G** eigenvectors calculated for selected Raman bands of $Bu_2(DCM)_2Tth$. Scaled and experimental (in parentheses) wavenumbers are given in cm^{-1}.*

Raman Spectrum in the Mid – Low Energy Region

The Fourier transform Raman spectrum recorded for $Bu_2(DCM)_2Tth$ in the 2400 – 400 cm^{-1} energy region is displayed in Figure 9 together with the theoretical B3LYP/6-31G** spectrum. Figure 10 sketches the eigenvectors associated with the most important features and Table 1 summarizes the peak frequencies for the main Raman bands.

In the experimental spectrum, the $\tilde{\nu}$(C≡N) vibration appears as an intense band at 2208 cm^{-1}. Theoretically, two normal modes calculated at 2238 and 2223 cm^{-1} are found to contribute to this band. The eigenvectors, which describe these modes, are the

Table 1. *Vibrational Raman frequencies (in cm^{-1}) measured for $Bu_2(DCM)_2Tth$ in solid state and in solution. $\Delta\tilde{\nu}$ corresponds to the difference (in cm^{-1}) between the frequency of the band at -150 °C and at +210 °C. The symbol (–) indicates that the measurement was not possible.*

Band	Assignment	CS_2	CH_2Cl_2	CH_3CN	$\Delta\tilde{\nu}$
2208	$\tilde{\nu}$(C≡N)	2212	2215	2217	+12
1512	$\tilde{\nu}(C_\beta{=}C_\beta)$	1516	1519	1519	+5
1493	$\tilde{\nu}(C_\beta{=}C_\beta)$	1495	1498	1498	+2
1460	$\tilde{\nu}(C_\alpha{=}C_{\alpha'})$, $\tilde{\nu}(C_\alpha{=}C_{sp^2})$	1469	1470	1470	+6
1379	ECC mode	1381	1388	1391	+10
1348	$\tilde{\nu}(C_\alpha{-}C_\beta)$	1346	1350	1351	+7
1246	$\tilde{\nu}(C_\alpha{-}C_\beta)$, $\tilde{\nu}$(C–CN)	1250	1253	1253	+4
1233	$\tilde{\nu}(C_\alpha{-}C_\beta)$	1233	1235	1236	+1
1176	$\tilde{\nu}$(C–C)	1178	1181	1182	+8
1143	$\tilde{\nu}$(C–C)	1145	1147	1147	+4
1138	$\tilde{\nu}$(C–C)	-	1138	1139	−2
1102	$\tilde{\nu}$(C–C)	1098	1100	1100	−2
1076	$\tilde{\nu}$(C–C)	1074	1075	1076	0
891	$\tilde{\nu}_s$(C–S)	–	893	–	–
838	$\tilde{\nu}_s$(C–S)	838	839	839	–
788	γ(C–H)	–	–	–	–
710	$\tilde{\nu}_s$(C–S)	711	–	712	+1
638	δ_{ring}	–	639	639	+1
577	δ_{ring}	–	578	579	–
562	δ_{ring}	563	563	–	–
549	δ_{ring}	550	550	550	–
456	δ_{ring}	454	455	454	–
426	γ_{ring}	–	426	–	–

same discussed above for the IR spectrum, but they now correspond to the in-phase symmetric and out-of-phase antisymmetric vibrations, respectively.

The experimental Raman spectrum in the 1600 – 400 cm^{-1} region is simpler than the IR spectrum (in spite of the absence of molecular symmetry). This observation is a common feature of polyconjugated molecules. Vibrational spectra of conjugated molecules are well-understood in the framework of the effective conjugation coordinate (ECC) theory .[9–11] This theory states the existence of a collective vibrational mode, ECC mode, which consists of a linear combination of ring C=C/C–C stretching vibrations. The associated frequency is an average of the strengths of the double and single bonds of the thiophene rings. In aromatic oligothiophenes, electronic interactions between adjacent thiophene rings give rise to the delocalization of the π electrons.[37] This results in a slight lengthening of the $C_\alpha{=}C_\beta$ bonds and in a shortening of the $C_\alpha{-}C_{\alpha'}$ and $C_\beta{-}C_\beta$ bonds, which form the conjugation pathway, as the length of the oligomer increases. For oxidized oligothiophenes, the $C_\alpha{=}C_\beta$ bonds of the originally aromatic structure lengthen, while the $C_\alpha{-}C_{\alpha'}$ and $C_\beta{-}C_\beta$ bonds shorten, as oxidation takes place. The structure evolves to a more quinoid-type geometry. Therefore, the frequency of the ECC mode (mainly made up of C=C stretching vibrations) downshifts with increasing the π-conjugation length of the oligomer or with increasing the quinoid character of the oligothiophene backbone.[17, 22, 23, 38]

The ECC mode usually corresponds to the strongest band of the Raman spectrum. The atomic motions involved in the ECC mode describe the evolution from an aromatic structure (HOMO orbital) to a quinoid structure (LUMO orbital) in aromatic oligothiophenes, and the opposite is true in quinoid oligothiophenes. This means that the ECC mode involves the easiest (less energetic) way to move atoms carrying out, at the same time, large changes of the electron density. This gives rise to the largest change of the molecular polarizability associated with a molecular vibration and, consequently, to the strongest Raman intensity for the ECC mode. The physical mechanism that sets up this phenomenon is known as the electron – phonon coupling mechanism.[39]

The Raman bands at 1379 and 1348 cm^{-1} are the most intense features of the spectrum and are calculated at 1392 and 1344 cm^{-1}, respectively. As sketched in Figure 10, the eigenvector of the mode at 1392 cm^{-1} corresponds to a totally symmetric $\tilde{\nu}$(C=C)/$\tilde{\nu}$(C–C) vibration that spreads over the whole terthienoquinoid spine, in which all double C-C bonds lengthen in-phase while all single C-C bonds shrink in-phase. This normal mode describes the evolution from a heteroquinoid structure to a heteroaromatic configuration of the π-conjugated backbone and, therefore, corresponds to the ECC mode. The band calculated at 1344 cm^{-1} arises from a $\tilde{\nu}(C_\alpha{-}C_\beta)$ stretching vibration, mainly located on the outermost rings (see Figure 10), and is coupled with $\tilde{\nu}(C_\alpha{=}C_{\alpha'})$ motions and in-plane δ(C–H) deformations of the thienyl C–H bonds.

For the unsubstituted $(DCM)_2Tth$ molecule, the ECC mode was assigned to the strongest Raman band observed at 1428 cm^{-1} and was calculated at 1420 cm^{-1} at the B3LYP/6-31G** level.[12a] The large downshift showed by the ECC mode in going from $(DCM)_2Tth$ to $Bu_2(DCM)_2Tth$ can be explained in terms of the changes induced by alkyl substitution on the molecular structure. B3LYP calculations predict that the attachment of butyl groups causes a lengthening of the two inter-ring $C_\alpha{=}C_{\alpha'}$ bonds (0.007 Å) and also of the $C_\alpha{-}C_\beta$ and $C_\beta{-}C_\beta$ bonds (0.011 and 0.021 Å, respectively) of the central thiophene ring. Since the frequency of the ECC vibration is largely determined by the stretching of these bonds, their lengthening upon alkyl substitution contributes to the downshift observed for this characteristic Raman vibration.

Bands at 1512, 1493, and 1460 cm^{-1} correlate with the theoretical features calculated around 1500 cm^{-1}, which are due to $\tilde{\nu}$(C=C) vibrations with different phases. The most intense band at 1512 cm^{-1} results from the vibration computed at 1517 cm^{-1}. This vibration describes a symmetric stretching of all C=C bonds, with the largest contributions corresponding to the $C_\beta{=}C_\beta$ bonds of the outermost thiophene rings (see Figure 10).

The weak – medium intensity Raman bands observed at 1246 and 1233 cm^{-1} are due to the normal modes calculated at 1230 and 1215 cm^{-1}. These modes describe the symmetric stretching of the $C_\alpha{-}C_\beta$ bonds vibrating in-phase within each thiophene ring and strongly coupled with the aliphatic $\delta(CH_2)$ vibrations of the butyl chains. The splitting into two bands results from the different structure of the thiophene rings. The band at higher frequencies involves the vibration of the outermost rings, while that at lower frequencies only implies the central ring, for which $C_\alpha{-}C_\beta$ bonds are longer. The bands at 1176 and 1138 cm^{-1} can be correlated with the theoretical bands at 1163 and 1124 cm^{-1} and are also attributed to symmetric $\tilde{\nu}(C_\alpha{-}C_\beta)$ vibrations but now coupled with in-plane δ(C–H) thienyl vibrations. Finally, the band

observed at 1076 cm^{-1} (calculated at 1062 cm^{-1}) implies the vibration of the central thiophene ring coupled with C–H deformation vibrations of the butyl chains.

Raman bands below 1000 cm^{-1} are not very interesting from the structural point of view because they are not directly related to the π-electron-conjugation pathway. This determines that the intensity of these bands is weak or very weak. Table 1 summarizes their Raman frequencies and their tentative assignment.

Solid-state Raman spectra of differently substituted α,α′-sexithiophenes in various oxidation states have been previously reported.[18] The Raman spectral pattern of the dication species consists of a strong scattering around 1415 – 1420 cm^{-1} and three medium – weak lines at about 1220, 1160, and 1050 cm^{-1}. This spectral profile correlates with the intense band at 1379 cm^{-1} and the medium – weak lines at 1246, 1143, and 1076 cm^{-1} observed here for the terthienoquinoid $Bu_2(DCM)_2Tth$ molecule. This close resemblance supports the hypothesis that $Bu_2(DCM)_2Tth$ can be viewed as a structural and electronic model of the dication or bipolaron species in oxidized aromatic oligothiophenes. The structural and electronic properties of the bipolaron species can be more thoroughly explored by studying quinoid systems such as $Bu_2(DCM)_2Tth$, which are completely free of chemical and conformational defects that are otherwise present in the doped polymer.

Raman Spectra in Solution and as Function of Temperature

Figure 11 compares the Raman spectra recorded for $Bu_2(DCM)_2Tth$ in CS_2, CH_2Cl_2, and CH_3CN solutions with that registered in the solid state. The frequencies of the most important spectral features are summarized in Table 1. Many works have previously analyzed the dependence of the electronic and vibrational spectra of aromatic oligothiophenes on the conformational flexibility of the oligothiophene backbone by studying the spectra in different media. The rotation around the C–C inter-ring bonds leads to the appearance of conformational rotamers, in which the π electron conjugation is less effective than in the planar conformer because of the lack of overlapping between the p_π orbitals of carbon atoms in adjacent rings.[40] This loss of π conjugation is reflected by the shifts observed for the spectral features in passing from the solid state to solution. For $Bu_2(DCM)_2Tth$, the Raman spectral patterns do not show any drastic change upon solution of the sample (see Figure 11 and Table 1). The maximum frequency shift is +12 cm^{-1} and is observed for the ECC mode. Unlike aromatic oligothiophenes, the data indicate that there is no coexistence of different conformers in solution for $Bu_2(DCM)_2Tth$. As expected, the molecules preserve the planarity upon solution because of the rigidity of the C=C inter-ring bonds that prevents from rotation around the thiophene rings.

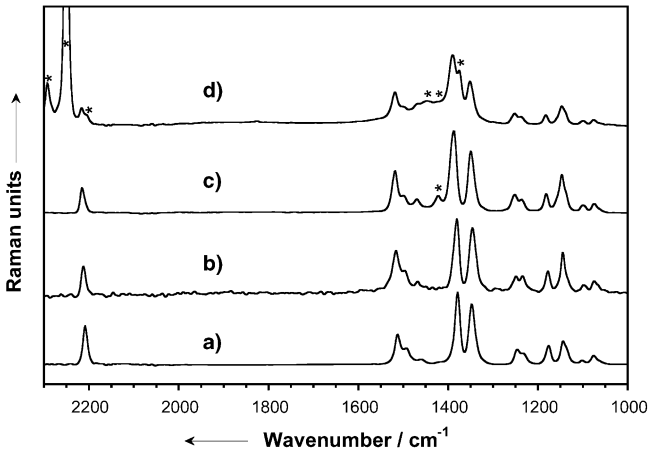

Figure 11. *FT-Raman spectra of $Bu_2(DCM)_2Tth$ recorded in solid state (a) and in CS_2 (b), CH_2Cl_2 (c), and CH_3CN (d) solutions over probe energies of 2300 – 1000 cm^{-1}. Asterisks denote solvent bands.*

As observed in Table 1, the Raman frequency of the $\tilde{\nu}$(C≡N) band upshifts by 4 cm^{-1} in passing from the solid state to CS_2 solution, and by another 5 cm^{-1} in passing to CH_3CN solution. The ECC mode recorded at 1379 cm^{-1} in the solid state also undergoes a total upshift of +12 cm^{-1} in going to CH_3CN solution. In the same way, the Raman bands assigned to $\tilde{\nu}$(C=C) vibrations at 1512, 1493, and 1460 cm^{-1} show upshifts of +7, +5, and +10 cm^{-1}, respectively. These frequency upshifts suggest a strengthening of the C≡N bonds and of the C=C double bonds, which form the π conjugation pathway, in passing from the solid state to solution and as the polarity of the solvent increases.

To study the influence of the solvent, the molecular geometry of the unsubstituted $(DCM)_2Tth$ trimer was reoptimized in the presence of acetonitrile using the polarized continuous model (PCM). This model considers the solvent as a continuous medium with a dielectric constant ε, and represents the solute by means of a cavity built with a number of interlaced atomic spheres.[41] Compared with the isolated molecule, the net charge supported by each $C(CN)_2$ group increases from −0.28*e* to −0.36*e* in CH_3CN solution. This indicates that, as expected, a more effective intramolecular charge transfer takes place from the terthiophene skeleton to the $C(CN)_2$ groups in CH_3CN solution, due to the polarity of the solvent. Calculations predict that the additional charge transfer leaves the C≡N bonds almost unaffected and shortens the C–CN bonds by 0.003 Å. The experimental upshift observed for the $\tilde{\nu}$(C≡N) vibration as the polarity of the solvent increases is, therefore, due to the shortening of the C–CN bonds, which vibrate together with the C≡N bonds. As for the oligothiophene backbone, both single and double CC bonds are slightly affected by the solvent. The terminal C_α=C_{sp^2} bonds lengthen by 0.003 Å and, at the same time, the inter-ring C_α=$C_{\alpha'}$ bonds, the C_β=C_β bond of the central ring, and the C_α–C_β bonds of the outer thiophene rings shorten by 0.001, 0.002, and 0.003 Å, respectively. As a whole, the C-C bonds that form the carbon skeleton are predicted to shorten, on average, by 0.0014 Å. Since both the single and the double C-C bonds are involved in the $\tilde{\nu}$(C=C) and $\tilde{\nu}$(C–C) vibrations, this shortening explains the fact that all the vibrations in the 1600 – 1000 cm^{-1} region (except for that at 1102 cm^{-1}) undergo a frequency upshift upon solution and as the polarity of the solvent increases.

The variable-temperature FT-Raman spectra of $Bu_2(DCM)_2Tth$ are shown in Figure 12. IR spectra are available upon request from the authors. The frequency changes ($\Delta\tilde{\nu}$) measured for the

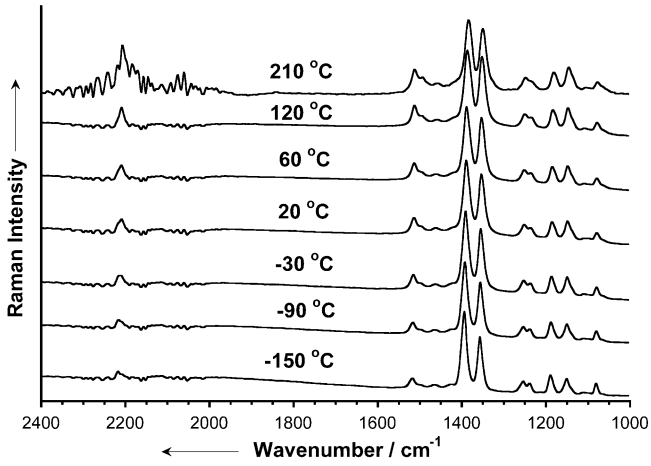

Figure 12. *FT-Raman spectra recorded at different temperatures for solid $Bu_2(DCM)_2Tth$ over probe energies of 2300 – 1000 cm^{-1}.*

Raman bands in going from the highest to the lowest temperature recorded are summarized in Table 1. The range of temperatures studied was from -150 to 210 °C (123 – 473 K). Intermediate spectra were recorded at -90, -30, 20, 60, and 120 °C. No drastic changes were noticed and the spectra reversibly recovered their profiles throughout the whole temperature range. No conformational distortion, neither in the oligothiophene backbone nor in the butyl chains, is therefore expected to take place. Frequency shifts of the IR and Raman bands, similar to those described above for the spectra in solution, are, however, obtained on going from the highest to the lowest temperature. The bands associated with the $\tilde{\nu}$(C=C) vibrations, as well as that corresponding to the $\tilde{\nu}$(C≡N) stretching, move to higher frequencies, as the temperature decreases. The Raman upshifts recorded for the $\tilde{\nu}$(C≡N) vibration ($+12$ cm^{-1}) and for the ECC mode ($+10$ cm^{-1}) are almost identical to those obtained in solution. As mentioned above, X-ray data for single crystals of $Bu_2(DCM)_2Tth$ revealed a π-dimerized structure.[5, 6] Furthermore, temperature-dependent thin-film and powder X-ray scattering show that the intermolecular separation in the π dimer expands with increasing temperature.[7] These slight modifications of the molecular packing (and, consequently, of the intermolecular interactions) can be the reason for the shifts observed in the vibrational spectra of solid $Bu_2(DCM)_2Tth$ as a function of temperature.

3. Conclusions

The molecular and electronic structures of the end-capped bis(dicyanomethylene)terthiophene $Bu_2(DCM)_2Tth$ have been investigated using UV/Vis, infrared, and Raman spectroscopies together with DFT B3LYP/6-31G** calculations. The terthiophene backbone exhibits a heteroquinoid structure similar to that predicted for aromatic oligothiophenes in the dication or bipolaron state. Both theoretical calculations and IR data indicate that an electron density transfer of about 0.25 – 0.30*e* takes place from the central terthiophene moiety to each $C(CN)_2$ group in the electronic ground state. This intramolecular charge transfer gives rise to an electron-deficient oligothiophene backbone, which explains the fact that $Bu_2(DCM)_2Tth$ shows a much more efficient n-channel conduction (over the p-channel transport) in thin film transistors.[6]

The heteroquinoid structure of $Bu_2(DCM)_2Tth$ is characterized by a strong low-energy absorption band (650 – 700 nm) that is assigned to the HOMO → LUMO $S_0 \rightarrow S_1$ electronic transition. The calculations show that the absorption originates in the $\pi-\pi^*$ transition of the terthiophene backbone and that no significant intramolecular charge transfer to the end-capping $C(CN)_2$ groups takes place upon excitation. The absorption band undergoes a hypsochromic shift in passing from the solid state to solution and as the polarity of the solvent increases; this suggests that the energy stabilization (due to solvent effects) is larger for the electronic ground state.

The infrared and Raman spectra have been comprehensively assigned on the basis of theoretical calculations. The most intense band of both spectra corresponds to a $\tilde{\nu}$(C=C)/$\tilde{\nu}$(C–C) vibration spreading over the whole terthienoquinoid backbone. The Raman vibration (1379 cm^{-1}) is assigned to the so-called ECC mode, which averages the collective motion of the C=C and C–C bonds describing the evolution from the quinoid structure displayed by the molecule to an aromatic structure. The Raman spectral pattern obtained for $Bu_2(DCM)_2Tth$ correlates with those previously reported for aromatic oligothiophenes in the dication or bipolaron state, thus supporting the similar molecular and electronic structures of both systems. The Raman spectra recorded in solution show that a more effective intramolecular charge transfer takes place for the ground state of $Bu_2(DCM)_2Tth$ in solution and as the polarity of the solvent increases. Finally, the sizeable shifts observed as a function of temperature for the solid-state vibrational spectra reflect the changes induced by temperature on the molecular packing.

4. Experimental and Computational Details

The synthesis and purification of $Bu_2(DCM)_2Tth$ were described elsewhere.[5] Spectra in the UV/Vis region (350 – 900 nm) were recorded at room temperature with an Ocean Optics spectrometer equipped with a Silicon detector. Spectra in solution were registered in non-degassed media. FT-infrared measurements were obtained with a Perkin-Elmer 1760 X spectrometer. The oligomer was ground to a powder and pressed in KBr pellets. All spectra were collected using a resolution of 2 cm^{-1} and an average of 50 scans was obtained. Interference from atmospheric water vapor was minimized by purging the instrument for 10 – 15 min with dry argon before data collection. Raman measurements were performed with the FRA/106 S modulus of a FT-Raman Bruker Equinox 55 FTIR interferometer, which operates upon a near infrared diode-pumped Nd:YAG laser with an excitation wavelength of 1064 nm. Signal detection was carried out by means of a germanium detector, which works at liquid nitrogen temperature. UV/Vis and Raman spectra of the solutions were carried out in carbon disulfide (CS_2), dichloromethane (CH_2Cl_2),

carbon tetrachloride (CCl_4) and acetonitrile (CH_3CN) purchased from Sigma-Aldrich (HPLC quality).

Variable temperature experiments were carried out using a Specac P/N 21 525 cell provided with interchangeable pairs of NaCl or quartz windows for transmission studies. The variable temperature cell consists of a surrounding vacuum jacket (0.5 Torr), which contains a combination of a refrigerant dewar and a heating block as the sample holder. The cell was equipped with a Copper-Constanton thermocouple (for temperature monitoring purposes) that allows any temperature from -150 to $+210\,^{\circ}C$ (123 – 483 K) to be achieved. The samples were inserted into the heating block part or the dewar/cell holder assembly in the form of KBr pellets. The spectra were recorded after waiting for thermal equilibrium at the sample, which required 20 min for every increment of 10 °C.

DFT calculations were carried out using the A.7 revision of the GAUSSIAN 98 program package[42] running on SGI Origin 2000 computers and IBM RS/6000 workstations. All calculations, which include: geometry optimizations, electronic excitation energies, and vibrational spectra, were performed on isolated systems using the Becke's three parameter B3LYP exchange-correlation functional.[43] The 6-31G** basis set[44] was chosen as a compromise between accuracy and applicability to large molecules. Vertical excitation energies were computed for the fifteen lowest-energy electronic excited states by using the time-dependent DFT (TDDFT) approach.[45–47] This approach has been widely used to study the electronic spectra of large π-conjugated systems such as polyenes,[48] polycyclic aromatic hydrocarbons,[49, 50] fullerenes,[51] oligomers of α-thiophenes, para-phenylenes, and para-phenylenevinylenes,[52] porphyrin-type macrocycles and oligomers,[53, 54] etc. Standard hybrid functionals such as BLYP and B3LYP have shown to provide excitation energies that are roughly within 0.3 eV of the experimental data. Despite these encouraging results, the TDDFT approach should be used with caution, because the excitation energies can be affected by quite different errors. Overestimations/underestimations in the 0.4 – 0.7 eV range are not uncommon,[48, 49e,f] and they can lead to wrong assignments when trying to provide a full interpretation of the electronic spectrum.[55]

The calculated harmonic vibrational frequencies were scaled down uniformly by a factor of 0.96 as recommended by Scott and Radom.[56] All the theoretical vibrational data quoted in the text are thus scaled values. The theoretical infrared and Raman spectra were obtained by convoluting the scaled frequencies with Gaussian functions (10 cm^{-1} width at the half maximum). The height of the Gaussians was determined from the IR intensities and Raman scattering activities calculated for the IR- and Raman-active normal modes, respectively. The IR intensities were calculated from the dipole moment derivatives with respect to normal coordinates, while polarizability derivatives for Raman activities were obtained using numerical differentiation of the analytical dipole moment derivatives with respect to the applied electric field. The relative intensity of the most intense line appears to be theoretically overestimated by comparison with experimental IR and Raman bands.

Acknowledgements

Research at the Universities of Valencia and Málaga was supported by the Ministerio de Ciencia y Tecnología (MCyT) of Spain through the projects BQU2002-10656-E, BQU2003-05111, and BQU2000-1156. B.M. is grateful to the Ministerio de Educación, Cultura y Deporte of Spain for a doctoral grant. We are also indebted to Junta de Andalucía (Spain) for funding our research group (FQM-0159). J.C. is grateful to the Ministerio de Ciencia y Tecnología of Spain for a Ramón y Cajal position of Chemistry at the University of Málaga. Work at the University of Minnesota was supported by the National Science Foundation.

Keywords: density functional calculation · electronic spectroscopy · oligothiophenes · thin films · vibrational spectroscopy

[1] a) G. Horowitz, D. Fichou, X. Z. Peng, F. Garnier, *Solid State Commun*. **1989**, *72*, 381; b) D. Fichou, *J. Mater. Chem*. **2000**, *10*, 571.
[2] a) L. Wenjie, H. E. Katz, A. J. Lovinger, J. G. Laquindanum, *Chem. Mater.* **1999**, *11*, 458; b) H. E. Katz, Z. Bao, S. L. Gilat, *Acc. Chem. Res*. **2001**, *34*, 359.
[3] J. Cornil, J. P. Calbert, J. L. Brédas, *J. Am. Chem. Soc*. **2001**, *123*, 1250.
[4] a) J. Cornil, D. Beljonne, J. P. Calbert, J. L. Brédas, *Adv. Mater.* **2001**, *13*, 1053; b) J. Cornil, D. Beljonne, D. A. dos Santos, J. P. Calbert, J. L. Brédas, *Acc. Chem. Res.* **1999**, *32*, 267; c) J. Cornil, J. P. Calbert, D. Beljonne, R. Silbey, J. L. Brédas, *Adv. Mater.* **2000**, *12*, 978.
[5] T. M. Pappenfus, J. D. Raff, E. J. Hukkanen, J. R. Burney, J. Casado, S. M. Drew, L. L. Miller, K. R. Mann, *J. Org. Chem*. **2002**, *67*, 6015.
[6] T. M. Pappenfus, R. J. Chesterfield, C. D. Frisbie, K. R. Mann, J. Casado, J. D. Raff, L. L. Miller, *J. Am. Chem. Soc*. **2002**, *124*, 4184.
[7] R. J. Chesterfield, C. R. Newman, T. M. Pappenfus, P. C. Ewbank, M. H. Haukaas, K. R. Mann, L. L. Miller, C. D. Frisbie, *Adv. Mater.* **2003**, *15*, 1278.
[8] P. R. L. Malefant, C. D. Dimitrakopoulos, J. D. Gelorme, L. L. Kosbar, T. O. Graham, A. Curioni, W. Andreoni, *Appl. Phys. Lett.* **2002**, *80*, 2517.
[9] C. Castiglioni, J. T. López Navarrete, M. Gussoni, G. Zerbi, *Solid State Commun*. **1988**, *65*, 625.
[10] G. Zerbi, C. Castiglioni, J. T. López Navarrete, B. Tian, M. Gussoni, *Synth. Met*. **1989**, *28*, D359.
[11] G. Zerbi, M. Gussoni, C. Castiglioni in *Conjugated Polymers* (Eds.: J. L. Brédas, R. Silbey), Kluwer Academic Publishers, Dordrecht, **1991**, p. 435.
[12] a) V. Hernández, S. Hotta, J. T. López Navarrete, *J. Chem. Phys*. **1998**, *109*, 2543; b) J. Casado, L. L. Miller, K. R. Mann, T. M. Pappenfus, H. Higuchi, E. Ortí, B. Milián, R. Pou-Amérigo, V. Hernández, J. T. López Navarrete, *J. Am. Chem. Soc*. **2002**, *124*, 12 380.
[13] V. Hernández, S. Calvo Losada, J. Casado, H. Higuchi, J. T. López Navarrete, *J. Phys. Chem. A* **2000**, *104*, 661.
[14] V. Hernández, J. Casado, F. J. Ramírez, G. Zotti, S. Hotta, J. T. López Navarrete, *J. Chem. Phys.* **1996**, *104*, 9271.
[15] a) J. Casado, S. Hotta, V. Hernández, J. T. López Navarrete, *J. Phys. Chem. A.* **1999**, *103*, 816; b) V. Hernández, J. Casado, F. J. Ramírez, L. J. Alemany, S. Hotta, J. T. López Navarrete, *J. Phys. Chem.* **1996**, *100*, 289; c) V. Hernández, H. Muguruma, S. Hotta, J. T. López Navarrete, *J. Phys. Chem.* **2000**, *104*, 735.
[16] E. Agosti, M. Rivola, V. Hernández, M. Del Zoppo, G. Zerbi, *Synth. Met*. **1999**, *100*, 101.
[17] J. Casado, V. Hernández, S. Hotta, J. T. López Navarrete, *J. Chem. Phys*. **1998**, *109*, 10 419.
[18] a) J. Casado, V. Hernández, S. Hotta, J. T. López Navarrete, *Adv. Mater.* **1998**, *10*, 1458; b) J. Casado, H. E. Katz, V. Hernández, J. T. López Navarrete, *J. Phys. Chem. B* **2002**, *106*, 2488; c) J. Casado, L. L. Miller, K. R. Mann, T. M. Pappenfus, V. Hernández, J. T. López Navarrete, *J. Phys. Chem. B* **2002**, *106*, 3597.
[19] R. Taylor, O. Kennard, *J. Am. Chem. Soc*. **1982**, *104*, 5063.
[20] Differences between the B3LYP6-31G** results obtained for the C_2 and C_s structures have maximum values of 0.0002 Å for bond distances, 0.01 eV for electronic excitation energies, and 2 cm^{-1} for harmonic vibrational frequencies.
[21] S. Hotta, K. Waragai, *J. Mater. Chem*. **1991**, *1*, 835.
[22] D. D. Graf, R. G. Duan, J. P. Campbell, L. L. Miller, K. R. Mann, *J. Am. Chem. Soc.* **1997**, *119*, 5888.
[23] D. D. Graf, J. P. Campbell, K. R. Mann, L. L. Miller, *J. Am. Chem. Soc.* **1996**, *118*, 5480.
[24] a) C. Alemán, L. Juliá, *J. Phys. Chem.* **1996**, *100*, 14 661; b) S. Irle, H. Lischka, *J. Chem. Phys.* **1997**, *107*, 3021; c) G. Moro, G. Scalmani, U. Cossentino, D. Pitea, *Synth. Met.* **1998**, *92*, 69.

[25] a) P. M. Viruela, R. Viruela, E. Ortí, J. L. Brédas, *J. Am. Chem. Soc.* **1997**, *119*, 1360; b) R. Liu, X. Zhou, H. Kasmai, *Spectrochim. Acta A* **1997**, *53*, 1241; c) J. A. Altmann, N. C. Handy, V. E. Ingamells, *Mol. Phys.* **1997**, *92*, 339.
[26] B. Milián, R. Pou-Amérigo, R. Viruela, E. Ortí, *Chem. Phys. Lett.* **2003**, *375*, 376.
[27] C. van Pham, A. Burkhardt, R. Shabana, D. D. Cunningham, H. B. Mark, H. Zimmer, *Phosph. Sulf. Silic.* **1989**, *46*, 153.
[28] K. Yui, Y. Aso, T. Otsubo, F. Ogura, *Bull. Chem. Soc. Jpn.* **1989**, *62*, 1539.
[29] D. A. Tozer, R. D. Amos, N. C. Handy, B. O. Roos, L. Serrano-Andrés, *Mol. Phys.* **1999**, *97*, 859.
[30] a) C. Jamorski, J. B. Foresman, C. Thilgen, H.-P. Lüthi, *J. Chem. Phys.* **2002**, *116*, 8761; b) C. Jamorski, H.-P. Lüthi, *J. Chem. Phys.* **2002**, *117*, 4146 and C. Jamorski, H.-P. Lüthi, *J. Chem. Phys.* **2002**, *117*, 4157.
[31] a) S. Hotta, K. Waragai, *J. Phys. Chem*. **1993**, *97*, 7427; b) W. Gebauer, M. Sokolowski, E. Umbach, *Chem. Phys.* **1998**, *227*, 33; c) J. Gierschner, H.-G. Mack, H.-J. Egelheaf, S. Schweizer, B. Doser, D. Oelkrug, *Synth. Met*. **2003**, *138*, 311.
[32] H. Higuchi, T. Nakayama, H. Koyama, J. Ojima, T. Wada, H. Sasabe, *Bull. Chem. Soc. Jpn.* **1995**, *68*, 2363.
[33] H. Higuchi, S. Yoshida, Y. Uraki, J. Ojima, *Bull. Chem. Soc. Jpn.* **1998**, *71*, 2229.
[34] a) P. Baüerle, U. Segelbacher, A. Maier, M. Mehring, *J. Am. Chem. Soc*. **1993**, *115*, 10217; b) P. Baüerle, U. Segelbacher, K. U. Gaudl, D. Huttenlocher, M. Mehring, *Angew. Chem.* **1993**, *105*, 125; *Angew. Chem. Int. Ed. Engl.* **1993**, *32*, 76.
[35] a) T. Takenaka, *Spectrochim. Acta A* **1971**, *27*, 1735; b) A. Girlando, C. Pecile, *Spectrochim. Acta A* **1973**, *29*, 1859; c) E. Faulques, A. Leblanc, P. Molini, M. Decoster, F. Conan, J. E. Guerchais, J. Sala-Pala, *Spectrochim. Acta A* **1995**, *51*, 805.
[36] M. S. Khatkale, J. P. Devlin, *J. Chem. Phys*. **1979**, *70*, 1851.
[37] V. Hernández, C. Castiglioni, M. Del Zoppo, G. Zerbi, *Phys. Rev.* B **1994**, *50*, 9815.
[38] J. Casado, L. L. Miller, K. R. Mann, T. M. Pappenfus, Y. Kanemitsu, E. Ortí, P. M. Viruela, R. Pou-Amérigo, V. Hernández, J. T. López Navarrete, *J. Phys. Chem. A* **2002**, *106*, 3872.
[39] B. Horovitz, *Phys. Rev. Lett*. **1981**, *47*, 1491.
[40] a) V. Hernández, J. T. López Navarrete, *J. Chem. Phys*. **1994**, *101*, 1369; b) V. Hernández, J. Casado, F. J. Ramírez, L. J. Alemany, S. Hotta, J. T. López Navarrete, *J. Phys. Chem*. **1996**, *100*, 289; c) E. Ortí, P. M. Viruela, J. Sánchez-Marín, F. Tomás, *J. Phys. Chem*. **1995**, *99*, 4955; d) N. DiCesare, M. Belletete, F. Raymond, M. Leclerc, G. Durocher, *J. Phys. Chem*. **1998**, *102*, 2700.
[41] a) S. Miertus, E. Scrocco, J. Tomasi, *Chem. Phys*. **1981**, *55*, 117; b) M. Cossi, V. Barone, R. Cammi, J. Tomasi, *Chem. Phys. Lett.* **1996**, *255*, 327; c) C. Amovilli, V. Barone, R. Cammi, E. Cancès, M. Cossi, B. Menucci, C. S. Pomelli, J. Tomasi, *Advances in Quantum Chem.* **1998**, *32*, 227.
[42] *Gaussian 98 (Revision A.7),* M. J. Frisch, G. W. Trucks, H. B. Schlegel, G. E. Scuseria, M. A. Robb, J. R. Cheeseman, V. G. Zakrzewski, J. A. Montgomery, R. E. Stratman, J. C. Burant, S. Dapprich, J. M. Millam, A. D. Daniels, K. N. Kudin, M. C. Strain, O. Farkas, J. Tomasi, V. Barone, M. Cossi, R.Cammi, B. Mennucci, C. Pomelli, C. Adamo, S. Clifford, J. Ochterski, G. A. Petersson, P. Y. Ayala, Q. Cui, K. Morokuma, D. K. Malick, A. D. Rabuck, K. Raghavachari, J. B. Foresman, J. Cioslowski, J. V. Ortíz, A. G. Baboul, B. B. Stefanov, G. Liu, A. Liashenko, P. Piskorz, I. Komaromi, R. Gomperts, R. L. Martín, D. J. Fox, T. Keith, M. A. Al-Laham, C. Y. Peng, A. Nanayakkara, C. González, M. Challacombe, P. M. W. Gill, B. Johnson, W. Chen, M. W. Wong, J. L. Andres, M. Head-Gordon, E. S. Replogle, J. A. Pople, Gaussian Inc., Pittsburgh, **1998**.
[43] A. D. J. Becke, *Chem. Phys*. **1993**, *98*, 1372.
[44] M. M. Francl, W. J. Pietro, W. J. Hehre, J. S. Binkley, M. S. Gordon, D. J. Defrees, J. A. Pople, *J. Chem. Phys.* **1982**, *77*, 3654.
[45] a) E. Runge, E. K. U. Gross, *Phys. Rev. Lett.* **1984**, *52*, 997; b) E. K. U. Gross, W. Kohn, *Adv. Quantum Chem.* **1990**, *21*, 255; c) E. K. U. Gross, C. A. Ullrich, U. J. Gossman in *Density Functional Theory* (Eds.: E. K. U. Gross, R. M. Driezler), Plenum Press, New York, **1995**, p. 149.
[46] M. E. Casida in *Recent Advances in Density Functional Methods, Part I* (Ed.: D. P. Chong), World Scientific, Singapore, **1995**, p. 155.
[47] W. Koch, M. C. Holthausen, *A Chemist's Guide to Density Functional Theory,* Wiley-VCH, Weinheim, **2000**.
[48] C.-P. Hsu, S. Hirata, M. Head-Gordon, *J. Phys. Chem. A* **2001**, *105*, 451.
[49] a) S. Hirata, T. J. Lee, M. Head-Gordon, *J. Chem. Phys*. **1999**, *111*, 8904; b) H. H. Heinze, A. Görling, N. Rösch, *J. Chem. Phys*. **2000**, *113*, 2088; c) J. L. Weisman, T. J. Lee, M. Head-Gordon, *Spectrochim. Acta A* **2001**, *57*, 931; d) S. Hirata, M. Head-Gordon, J. Szcsepanski, M. Vala, *J. Phys. Chem.* **2003**, *107*, 4940; e) S. Grimme, M. Parac, *ChemPhysChem* **2003**, *3*, 292; f) M. Parac, S. Grimme, *Chem. Phys.* **2003**, *292*, 11.
[50] T. M. Halasinski, J. L. Weisman, R. Ruiterkamp, T. J. Lee, F. Salama, M. Head-Gordon, *J. Phys. Chem*. A **2003**, *107*, 3660.
[51] R. Bauernschmitt, R. Ahlrichs, F. H. Heinrich, M. M. Kappes, *J. Am. Chem. Soc.* **1998**, *120*, 5052.
[52] a) A. Pogantsch, G. Heimel, E. Zojer, *J. Chem. Phys*. **2002**, *117*, 5921; b) G. R. Hutchison, M. A. Ratner, T. J. Marks, *J. Chem. Phys*. *A* **2002**, *106*, 10596; c) J. Casado, T. M. Pappenfus, L. L. Miller, K. R. Mann, E. Ortí, P. M. Viruela, R. Pou-Amérigo, V. Hernández, J. T. López Navarrete, *J. Am. Chem. Soc.* **2003**, *125*, 2524.
[53] a) S. J. A. van Gisbergen, A. Rosa, G. Ricciardi, E. J. Baerends, *J. Chem. Phys*. **1999**, *111*, 2499; b) K. A. Nguyen, R. Pachter, *J. Chem. Phys*. **2001**, *114*, 10757; c) M. Jaworska, G. Kazibut, P. Lodowski, *J. Phys. Chem*. *A* **2003**, *107*, 1339.
[54] Y. Yamaguchi, *J. Chem. Phys*. **2002**, *117*, 9668.
[55] R. Pou-Amérigo, P. M. Viruela, R. Viruela, M. Rubio, E. Ortí, *Chem. Phys. Lett.* **2002**, *352*, 491.
[56] A. P. Scott, L. Radom, *J. Phys. Chem*. **1996**, *100*, 16502.

Received: September 9, 2003 [F963]
Revised: December 5, 2003

